INTERIM REPORT

Advanced Magnetometer System

SERDP Project MR-2646

OCTOBER 2018

Dr. Rui Zhang
Dr. Rahul Mhaskar
Geometrics

SERDP
DOD ▪ EPA ▪ DOE

REPORT DOCUMENTATION PAGE	*Form Approved OMB No. 0704-0188*

1. REPORT DATE *(DD-MM-YYYY)*
22/10/2018

2. REPORT TYPE
SERDP Interim Report

3. DATES COVERED *(From - To)*
9/26/2016 - 9/26/2021

4. TITLE AND SUBTITLE
Advanced Magnetometer System

5a. CONTRACT NUMBER
16-C-0010

5b. GRANT NUMBER

5c. PROGRAM ELEMENT NUMBER

6. AUTHOR(S)
Dr. Rui Zhang
Dr. Rahul Mhaskar

5d. PROJECT NUMBER
MR-2646

5e. TASK NUMBER

5f. WORK UNIT NUMBER

7. PERFORMING ORGANIZATION NAME(S) AND ADDRESS(ES)
GEOMETRICS, INC.
2190 Fortune Drive
San Jose, CA, 95131

8. PERFORMING ORGANIZATION REPORT NUMBER
MR-2646

9. SPONSORING/MONITORING AGENCY NAME(S) AND ADDRESS(ES)
Strategic Environmental Research and Development Program (SERDP)
4800 Mark Center Drive, Suite 16F16
Alexandria, VA 22350-3605

10. SPONSOR/MONITOR'S ACRONYM(S)
SERDP

11. SPONSOR/MONITOR'S REPORT NUMBER(S)
MR-2646

12. DISTRIBUTION/AVAILABILITY STATEMENT
DISTRIBUTION STATEMENT A. Approved for public release: distribution unlimited.

13. SUPPLEMENTARY NOTES

14. ABSTRACT
Scalar magnetometers and Time-Domain Electromagnetic (TDEM) systems are proven and effective technologies used extensively in the field to detect, discriminate and classify unexploded ordnance (UXO). However, it has not been possible to simultaneously run both sensors in close vicinity of each other due to the interruption of the magnetometer operation by the EM pulses. We propose a method minimizing the EM pulse interruption by developing advanced digital signal processing (DSP) techniques to drive the scalar magnetometer. The method requires the angle information of the magnetic field, which cannot be obtained using commercial scalar magnetometers. In the first phase of the project, we demonstrate the capability of extracting the field angle information based on intrinsic operating parameters of the magnetometer. Better than 0.02° sensitivity can be achieved in angle measurement at the optimal orientation of the magnetic field with a measurement time of 100 ms. The demonstrated angle measurement shows that it is possible to achieve the fast tracking of the EM pulse with our advanced scalar atomic magnetometer system.

15. SUBJECT TERMS
Scalar Atomic Magnetometer, Time-Domain Electromagnetic System, Polar Angle, Angle Measurement, Digital Signal Processing

16. SECURITY CLASSIFICATION OF: a. REPORT	b. ABSTRACT	c. THIS PAGE	17. LIMITATION OF ABSTRACT	18. NUMBER OF PAGES	19a. NAME OF RESPONSIBLE PERSON
UNCLASS	UNCLASS	UNCLASS	UNCLASS	22	Rui Zhang
					19b. TELEPHONE NUMBER *(Include area code)* 408-954-0522

Standard Form 298 (Rev. 8/98)
Prescribed by ANSI Std. Z39.18

Contents

List of Figures

List of Acronyms

AOM – Acousto-optic Modulator
Cs – Cesium
DBR – Distributed Bragg Reflector
DC – Direct Current
DPLL – Digital Phase Locked Loop
DSP – Digital Signal Processing
EM – Electromagnetic
ESTCP – Environmental Security Technology Certification Program
FPGA -- Field-programmable Gate Array
FWHM – Full Width at Half Maximum
Hz – Hertz
kHz -- kilohertz
MFAM – MicroFabricated Atomic Magnetometer
ms – milli-second
nT – nanoTesla
pT – picoTesla
μs – micro-second
μT – microTesla
OD – Optical Density
PLL – Phase Locked Loop
SERDP – Strategic Environmental Research and Development Program
TDEM – Time-Domain Electromagnetic
UXO – Unexploded Ordnance
VCSEL – Vertical Cavity Surface Emitting Laser
3-D – Three-dimensional

List of Keywords

Scalar Atomic Magnetometer, Time-Domain Electromagnetic System, Polar Angle, Angle Measurement, Digital Signal Processing

2190 Fortune Drive, San Jose, CA 95131 USA • Tel (408) 954-0522 • Fax (408) 954-0902

Advanced Signal Extraction in Scalar Atomic Magnetometers

Abstract

Scalar magnetometers and Time-Domain Electromagnetic (TDEM) systems are proven and effective technologies used extensively in the field to detect, discriminate and classify unexploded ordnance (UXO). However, it has not been possible to simultaneously run both sensors in close vicinity of each other due to the interruption of the magnetometer operation by the EM pulses. We propose a method minimizing the EM pulse interruption by developing advanced digital signal processing (DSP) techniques to drive the scalar magnetometer. The method requires the angle information of the magnetic field, which cannot be obtained using commercial scalar magnetometers. In the first phase of the project, we demonstrate the capability of extracting the field angle information based on intrinsic operating parameters of the magnetometer. Better than 0.02° sensitivity can be achieved in angle measurement at the optimal orientation of the magnetic field with a measurement time of 100 ms. The demonstrated angle measurement shows that it is possible to achieve the fast tracking of the EM pulse with our advanced scalar atomic magnetometer system.

Project Objectives

The objective of the MR-2646 project is to enable the integration of miniature laser-pumped cesium magnetometers with TDEM systems by improving the magnetometer to function in presence of an EM transmitter. This project relates to MRSON-16-01, Detection, Classification, and Remediation of Military Munitions Underwater. By developing technologies necessary to integrate a magnetometer array with an advanced TDEM system, this project addresses sensor development, platform integration, and analysis methodologies necessary for efficient large-scale collection of field data during the detailed survey phase and particularly in an underwater environment.

Scalar atomic magnetometers rely on the resonant Larmor precession of atomic spins to measure the magnitude of the magnetic field [1]. A high-amplitude EM pulse can interrupt the magnetometer operation by collapsing the precession signal. It typically takes a few tens of milliseconds for the magnetometer to find the resonant Larmor frequency again. The recovery time can be greatly reduced, however, if the initial driving frequency is set to be close to the resonant Larmor frequency. This can be implemented using the advanced digital signal processing (DSP) solutions we have developed for driving the scalar magnetometer. The resonant Larmor frequency during the EM pulse can be calculated based on the vector sum of the EM pulse and the background magnetic field. The EM pulse at the location of the magnetometer can be calibrated and the magnitude of the background field measured by the scalar magnetometer. If the angle information about the background field can also be obtained, we will be able to implement the fast-recovery method of operating the scalar magnetometers in the presence of EM pulses.

Specific technical objectives are as follows:

1. Evaluate, through simulations and laboratory experiments, advanced methods of signal extraction in the scalar magnetometer instrument.
2. Implement advanced methods of operating the sensors to obtain rapid DC magnetometer measurements in the presence of a TDEM system.
3. Investigate the possibility of discrimination using DC magnetic measurements, probing in different directions, in a manner analogous to advanced TDEM systems.

This Interim Report addresses the first objective of the project and covers partially the second objective, more specifically implementing the advanced signal extraction methods in the sensor operation. This report addresses two questions: Whether the orientation information of the magnetic field can be extracted through the operation of our scalar atomic magnetometers? And if so, how accurate is the measurement of field orientation? The fast-recovery of the magnetometer operation after the EM pulse is not affected by the outcome of this report since no angle information is required. However, achieving magnetometer operation during the EM pulse, critical to objective 3, greatly depends on the accuracy of the angle measurement since it determines the estimated resonant Larmor frequency during the EM pulse. The typical full width at half maximum (FWHM) of the magnetic resonance in the magnetometer studied is about 1 kHz. If the estimated Larmor frequency is less than FWHM away from the true Larmor frequency, we expect the fast-recovery to work. We also expect the semi-DC pulse to be locally compensated to be less than one micro Tesla at the location of the magnetometer to minimize the heading error effect. Therefore, to achieve a resonant frequency error of less than 1 kHz, an angle measurement accuracy of better than 15° is required.

Technical Approach

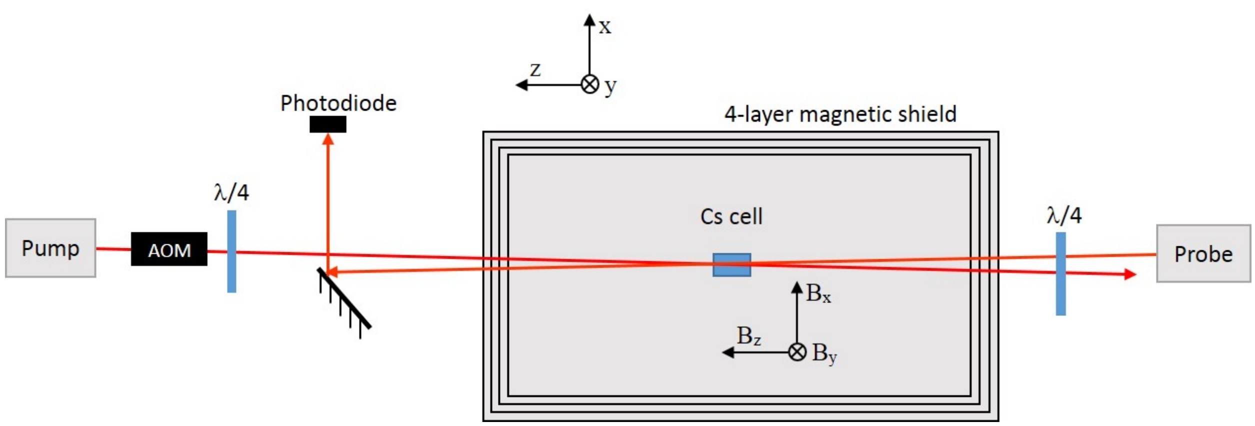

Figure 1 Schematic of the experimental setup of a bench-top scalar atomic magnetometer.

We use the bench-top scalar atomic magnetometer setup, shown schematically in Figure 1, to experimentally investigate the measurement concepts. A cuboid vapor cell containing Cs atoms is placed inside a 4-layer magnetic shield can. The cell is resistively heated to operating temperature. The pump and probe lights come from two Distributed Bragg Reflector (DBR) lasers and are circularly polarized with a quarter-wave-plate. The pump light is amplitude-modulated with an acousto-optic modulator (AOM). The angle between the two beams is about

1°. The fundamental operating principal of the magnetometer is based on the Bell-Bloom scheme [2]. The pump light periodically aligns atomic spins. The precession of the atomic spins in a magnetic field is detected by the counter-propagating probe beam. The transmitted probe light is detected and conditioned using electronics to determine the Larmor frequency and also control the AOM driving frequency. Inside the shield can, the magnetic field in x, y and z directions can be independently controlled.

1. DC transmission of the probe beam

a. Efficacy of the method

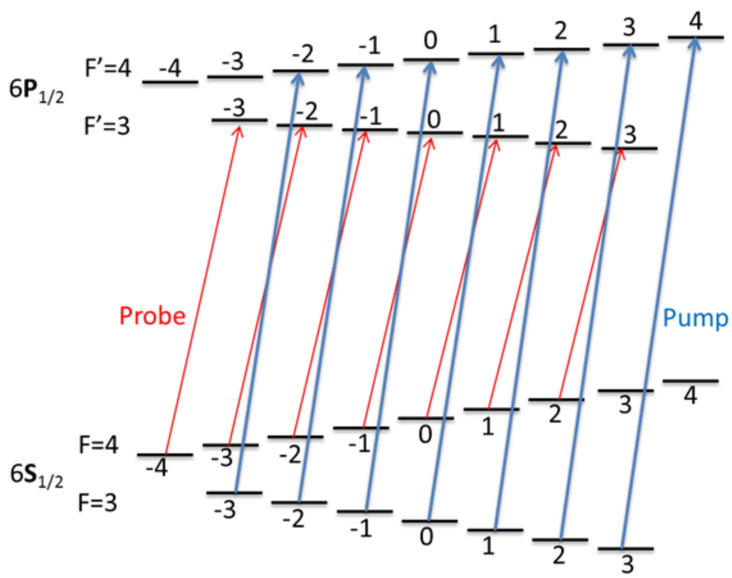

Figure 2 Transition diagram of the probe and pump beams.

The first method we investigate to measure magnetic field orientation is based on the DC transmission of the probe light. The transition diagram of a pump-probe atomic magnetometer based on the Bell-Bloom scheme [2] is shown in Figure 2. The probe light is circularly polarized, resonant with the |F=4>→|F'=3> transition of Cs D1 line. The two extreme magnetic sublevels of |F=4> ground state are dark states to the probe. Atoms in these states will not interact with probe photons. When the polar angle, θ (the angle between the magnetic field and the light) is 90°, atoms decaying into the dark states will escape quickly due to the Larmor precession. However, when the light and the magnetic field are aligned (polar angle at 0° or 180°), atoms decaying into the dark states get trapped. This decreases the optical density (OD) of the vapor. The OD is defined as OD = -log(P_{out}/P_{in}), where P_{in} and P_{out} are the input and output of the light power, respectively. We can write the effective OD for the probe light as $OD(\theta)=OD_0+OD_1*\sin^2\theta+OD_2*\sin^4\theta$. Then, the transmitted probe intensity, I, satisfies the following equation,

$$I(\theta) = I_0 e^{-OD(\theta)} = I_0 e^{-OD_0} e^{-OD_1 sin^2\theta - OD_2 sin^4\theta} . \quad (1)$$

The transmission dependence of the probe light on θ is studied with the experimental setup shown in Figure 1. We first rotate the magnetic field in the x-z plane while keeping its magnitude constant. The transmitted probe beam is detected by a photodiode and the photo current, amplified by a trans-impedance amplifier, is recorded. The DC photodiode signal as a function of θ is shown as dots in Figure 3. The magnetometer is operating during the measurement.

According to Equation (1), we fit the data with the following function:

$$y = A * \exp\left[-B * sin^2(\theta - \theta_0) - C * sin^4(\theta - \theta_0)\right]. \qquad (2)$$

An offset in the polar angle, θ_0, is added to the fitting function in order to compensate for any systematic error in θ. The fitting result is plotted as the red curve in Figure 3. As seen, the theoretical model agrees well with the experimental data. We also rotate the magnetic field in planes other than x-z and obtain similar results.

The probe DC signal only depends on the polar angle of the magnetic field, not its magnitude. To verify this, we conduct similar experiments in magnetic fields of different strengths. The results are shown in Figure 4. As expected, the magnitude of the magnetic field does not affect the transmitted probe light DC level. The slight disagreement is likely due to the error in the polar angle. Even though we can generate precise Bx, By and Bz with state-of-the-art current sources, there may be changing stray magnetic fields inside the shield can, which affect the actual polar angle during the measurement. The cell temperature is not actively stabilized in the experiments conducted in the benchtop setup, possibly contributing to error seen in Figure 4.

Overall, according to our experimental results presented above, the probe DC transmission signal can be used to measure the polar angle of the magnetic field.

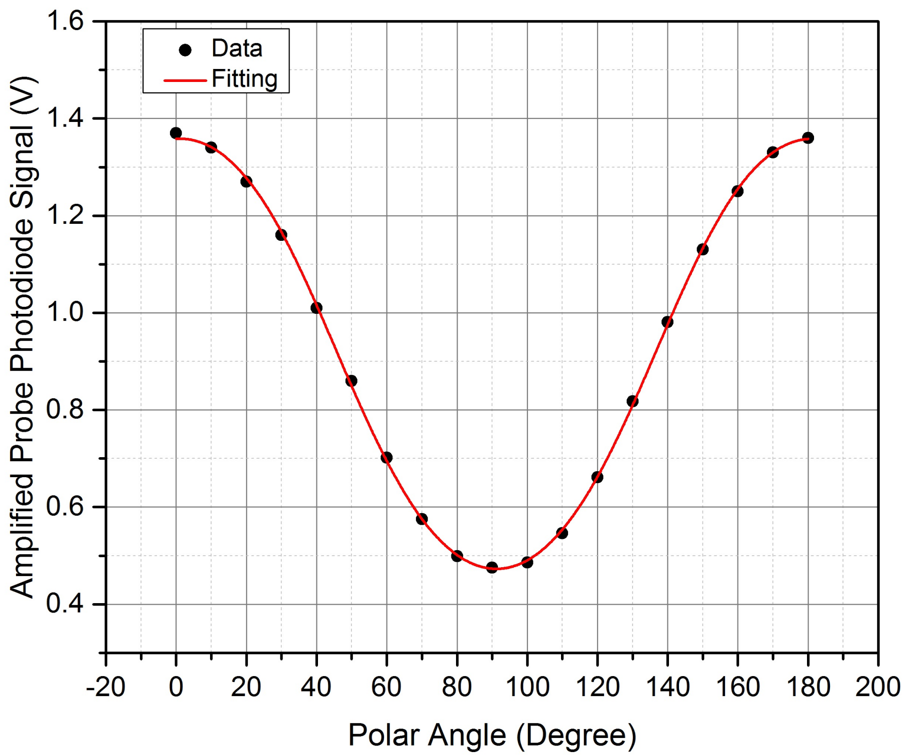

Figure 3 Transmitted probe light DC signal as a function of the polar angle. The magnetic field vector is in the x-z plane. The red curve is the fitting to the experimental data, represented by dots.

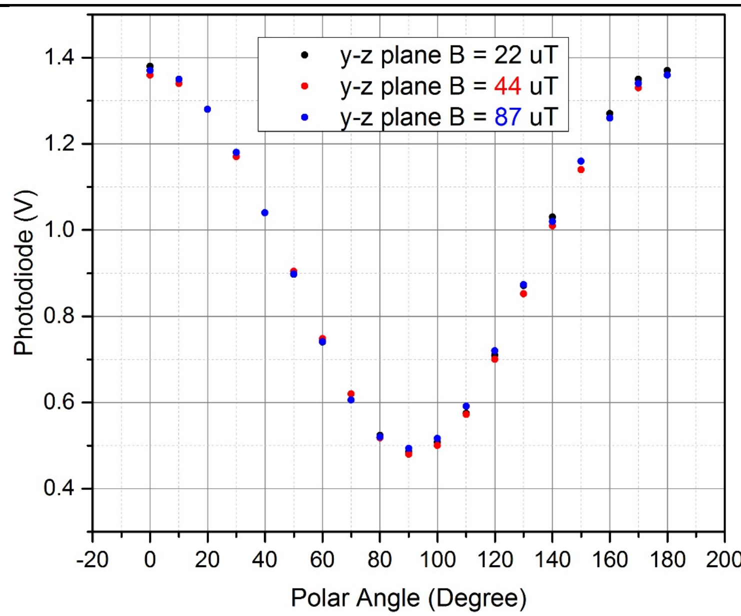

Figure 4 Transmitted probe DC as a function of polar angle of the magnetic field. Black, red and blue dots represent results at B of 22 µT, 44 µT and 87 µT, respectively. The slight difference is likely due to the inaccuracy of polar angles and the fluctuation in cell temperature.

b. Noise in the Polar Angle Measurement

To investigate the noise in the polar angle measurement using the probe DC transmission, we record the signal for 5 minutes and calculate its Allan Deviation [3]. The Allan Deviation at 50° polar angle is shown in Figure 5. As seen, with about 0.1 second integration time (10 Hz sample rate), the Allan Deviation of the probe DC is less than 0.1 mV. At 50° polar angle, the DC/polar angle calibration slope according to Figure 4 is roughly 16mV/degree. Therefore, a 0.1 mV variation in the probe DC will lead to about 0.006° noise in the polar angle measurement, which is very sensitive. In fact, even at 88° polar angle, the slope is still 0.9mV/degree. A sensitivity of 0.1° in the polar angle can still be achieved with the 0.1 mV noise in the probe DC.

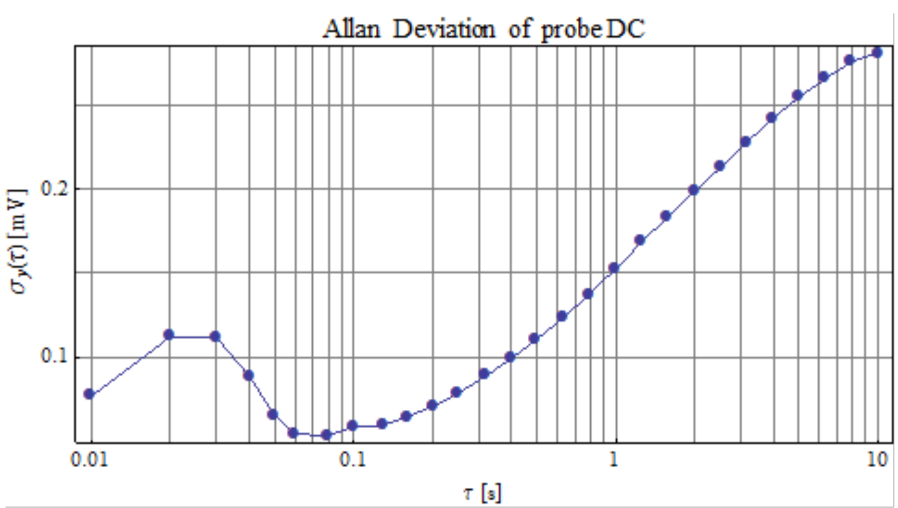

Figure 5 Allan Deviation of the probe DC transmission at 50° polar angle.

c. Dynamic Response of the Polar Angle Measurement

So far, all the measurements discussed above were done in steady state where the magnetic field does not change its relative direction or magnitude. In most mobile applications, however, the polar angle of the magnetic field will change. Here we present the dynamic response of the probe DC method to a changing magnetic field.

As we discussed before, the probe DC signal is independent of the magnitude of the magnetic field. We further confirm this by monitoring the DC signal while applying a magnitude change to the magnetic field. No change is observed in the DC signal.

In order to generate a sudden change in the direction of the B field, we initially apply fields in both x and z direction, Bx = 20 μT and Bz = 20 μT. At t = 5 ms, Bx is switched off in less than 50 μs. Figure 6 shows the response of the probe DC signal when the Bx is switched off. The curve cannot be modeled with an exponential function with a single time constant. Instead, three time constants are required, with the longest time constant being 950μs. Hence, the probe DC signal responds to a change in the B field direction with bandwidth greater than 100 Hz. Considering that it is unlikely that the polar angle of the B field will vary at a rate beyond 100 Hz in practical applications, the fundamental dynamic response of the probe DC method is not expected to limit the B field angle measurements.

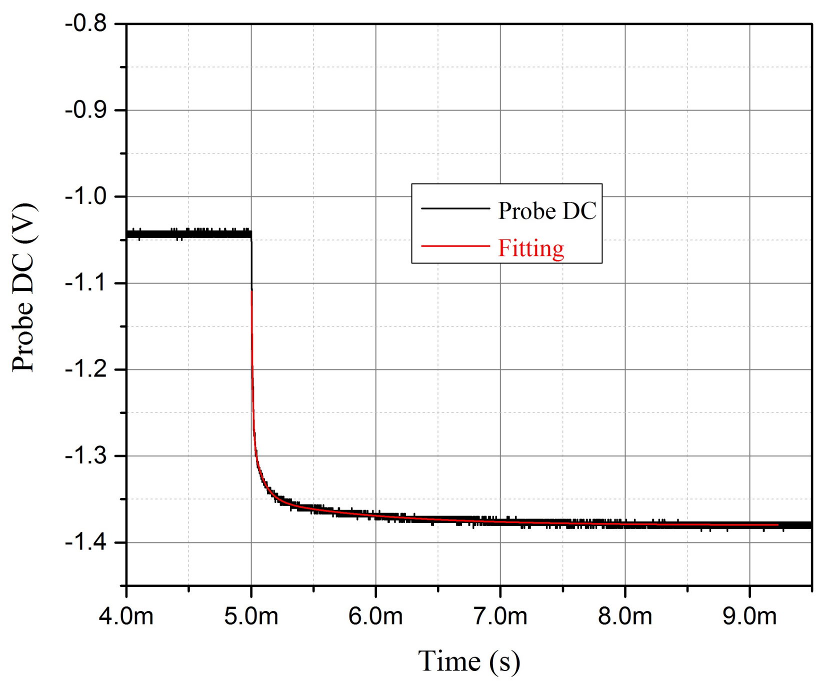

Figure 6 Dynamic response of the probe DC to a sudden change of the B field direction. Polar angle changes from 45° to 0° at t = 5 ms.

d. Discussion

There are two major issues with the polar angle measurement using the probe DC method. First, the probe DC signal is symmetric with respect to $\theta = 90°$. Therefore, based on the probe DC signal only, the polar angle is not unique. The other problem is that the response of the probe DC to θ around 90° is flat, as seen in Figure 3, leading to a poor sensitivity of this method. For

θ close to 0° or 180°, the sensitivity is also poor. However, this is the dead zone for the magnetometer. In practice, the magnetometer would never be operated close to this orientation.

2. Probe Light Shift

a. Efficacy of the Method

To overcome the issues observed with the probe DC method, we consider the following supplementary method. Circularly polarized light causes a slight shift of energy levels of atomic ground states, equivalent to a fictitious magnetic field being applied along the light propagation direction [4]. The total effective magnetic field, which is measured by the magnetometer, is given by the vector sum of real magnetic field $\boldsymbol{B}$ and the fictitious magnetic field $\boldsymbol{B_k}$. In general, $B_k \ll B$. The effective magnetic field can be approximated by $B + B_k cos\theta$. B_k depends on the wavelength of the light. If the probe laser optical wavelength is dithered at a frequency f by adding a small oscillating current to the laser drive current, B_k will also develop an oscillating component with the same frequency f, $B_k{=}B_k^0{+}B_k^1{*}\sin(2\pi ft)$. When the measured magnetic field is demodulated at the frequency f, component $B_k^1 cos\theta$ can be extracted. Since B_k^1 is a constant to the first order, the value of $B_k^1 cos\theta$ gives us a measurement of θ.

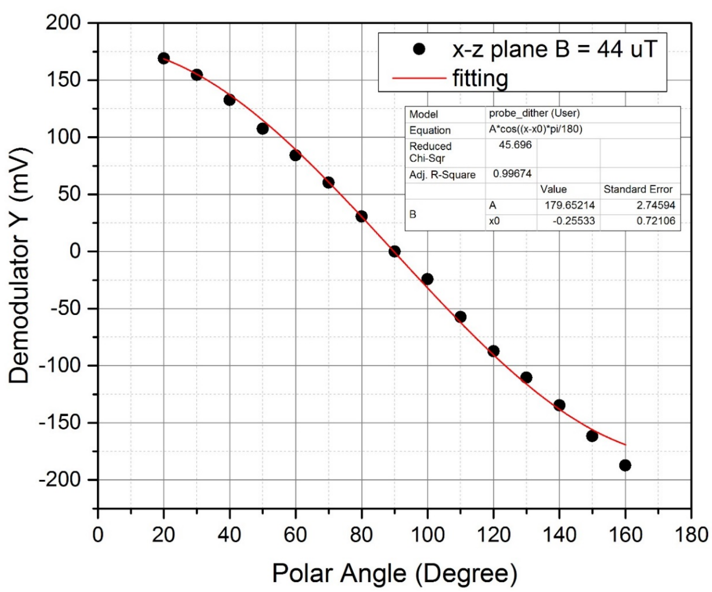

Figure 7 Response of the light-shift induced magnetic field to the polar angle. The pseudo magnetic field is measured by demodulating the magnetometer output at the frequency dithering the probe current. Y component of the demodulator output is plotted as a function of polar angle.

To implement this method, we inject a 2 kHz signal in the probe laser current. The signal dithers the laser wavelength by about 0.1 pm. We then demodulate the magnetometer output at the 2 kHz dither frequency. The phase of the demodulator is set such that the y-component output is maximized at 160° polar angle. We rotate the magnetic field (with the same magnitude) in both x-z and y-z plane. At each polar angle, the y-component output is recorded. The result in x-z plane is shown as black dots in Figure 7. As discussed previously, the data should follow the function $y{=}A cos(\theta - \theta_0)$. Here θ_0 is added to compensate for any systematic error in θ. A nonlinear fit of the function to the experimental data yields a good agreement between the theory and the experiment. The fitting result is plotted as the red curve. The discrepancies are mostly due to inaccuracies in setting the actual polar angle. We obtain similar results in the y-z plane.

b. Noise in the Polar Angle Measurement

We record the y-component output for 5 mins and calculate its Allan Deviation. The Allan Deviation for 90° polar angle is shown in Figure 8. As seen, with 0.1s integration time, the Allan Deviation is about 0.4 mV for the y component. According to Figure 7, around 90° polar angle, the slope y/polar is about 2.5 mV/degree. Therefore, a 0.4 mV variation in the y component will lead to about 0.2° noise in the polar angle.

c. Dynamic Response of the Polar Angle Measurement

The dependence of the y-component on the polar angle is simply due to the projection of the light-shift induced magnetic field onto the main magnetic field. The response of the projection to the polar angle change is expected to be instantaneous.

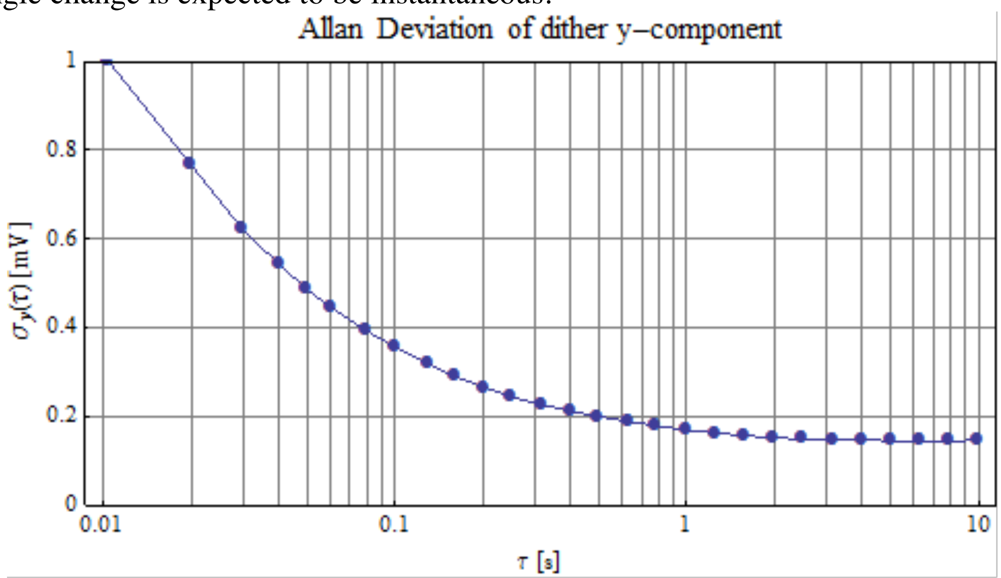

Figure 8 Allan Deviation of the y-component output at 90° polar angle.

d. Discussion

This method relies on the measurement of the magnetic field. When the magnetometer is orientated close to dead zone, the increased noise in the magnetometer output leads to significant increase in noise in the polar angle measurement.

3. Azimuthal Angle Measurement

If two scalar magnetometers are used, we can extract some information about the azimuthal angle as well. Assuming that two probes in the magnetometers are aligned as shown in Figure 9 and the relative polar angles, θ_1 and θ_2, are calculated based on the methods presented above, then the azimuthal angle of the magnetic field, φ, satisfies the following equation:

$$\cos\varphi = \frac{\cos\theta_2 - \cos\theta_1 \cos\theta_0}{\sin\theta_1 \sin\theta_0}. \quad (3)$$

Here θ_0 is the angle separation between the two probes. For θ_0 = 90°, Equation (3) can be simplified. The azimuthal angle is then calculated to be $\varphi = arccos(\cos\theta_2/\sin\theta_1)$. Note that *arccosine* is only defined between 0° and 180°. The azimuthal angle is still undetermined between φ and 360°- φ.

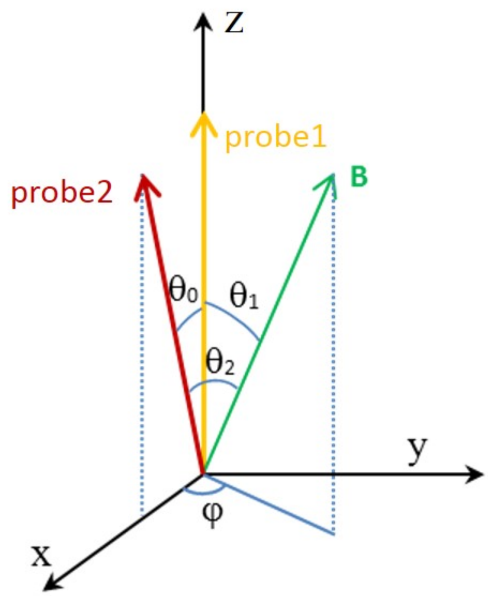

Figure 9 Schematics showing the relative directions of two probes and the magnetic field. The azimuthal angle of the magnetic field can be calculated based on the two polar angles and the angle separation between the two probes.

Results and Discussion

In the MFAM™ sensor, we replaced the DBR lasers shown in Figure 2 with vertical cavity surface emitting lasers (VCSELs). The optical wavelength of the VCSELs can be dithered at the Larmor frequency through laser current modulation, thus eliminating the need for AOMs. With these changes, we were able to integrate the bench top magnetometer into a sensor package less than 20 cubic centimeters in volume. All signals generated by the sensor are analyzed by a field-programmable gate array (FPGA). The DSP programmed within the FPGA records the probe DC signal and calculates the demodulated probe light-shift amplitude. The MFAM sensor outputs both the probe DC level and the probe light-shift amplitude at a rate of 100 samples per second. Note that the magnetic field output of the MFAM is still at 1000 samples per second. In the following, we use the MFAM sensors to investigate the field angle measurements.

1. Polar Angle Measurement

a. Characterization of the Probe DC Method

We first verify the response of the sensor probe DC level to the change of polar angle. The results are shown in Figure 10. A fit of Equation (2) to the experimental data is also shown as the red curve. As seen, the data agrees well with the theoretical model. Based on the fitting parameters, a look-up table of probe DC vs polar angle is generated. In the polar angle measurement, after the probe DC value is measured, the closest table element is found and the polar angle is interpolated linearly.

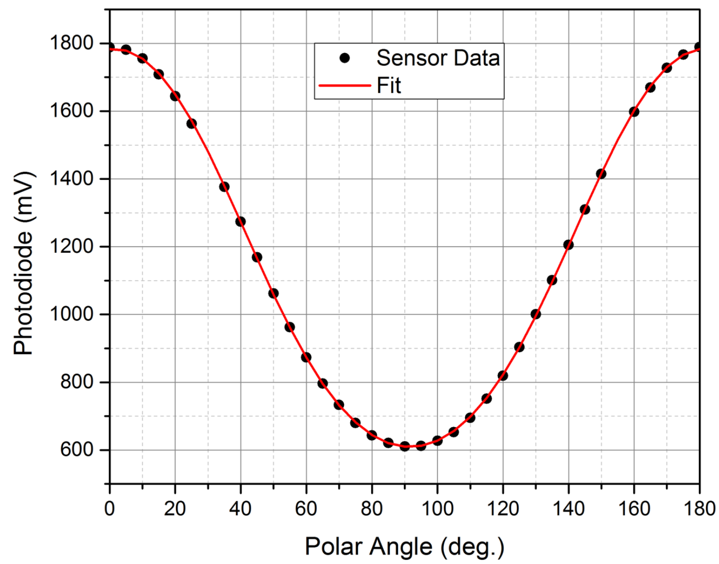

Figure 10 Probe DC output of a MFAM sensor as a function of polar angle (black dots). The red curve is a fit of Equation (2) to the data.

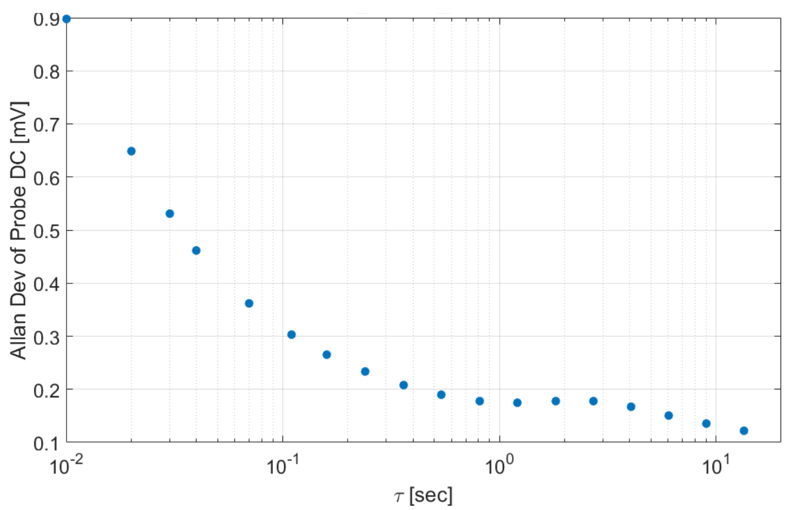

Figure 11 The Allan deviation of the probe DC output.

We also measure the Allan Deviation of the probe DC output with the polar angle set at about 45°. The result is shown in Figure 11. With an integration time of over 100 ms, the deviation of the probe DC drops below 0.3 mV. Combined with the slope of the curve in Figure 10 of about 0.05 degree/mV around 45° polar angle, the most sensitive region of the angle measurement should have resolution better than 0.02°.

The bandwidth of the polar angle measurement based on the probe DC is also investigated. We set the polar angle to about 60°. A small oscillating field is added perpendicular to the probe. As a result, the total polar angle is changed by a couple of degrees at the same frequency as the oscillating field. We fix the oscillating field amplitude and change its frequency.

The amplitude of the measured oscillating polar angle is recorded as a function of the driving frequency. The gain of the polar angle measurement at a certain frequency is calculated as the normalized amplitude relative to that at 1 Hz. The result is plotted in Figure 12. As seen, the bandwidth of angle measurement technique based on probe DC level detection is well above 50 Hz and is currently limited by the DC level reporting rate of 100 samples per second.

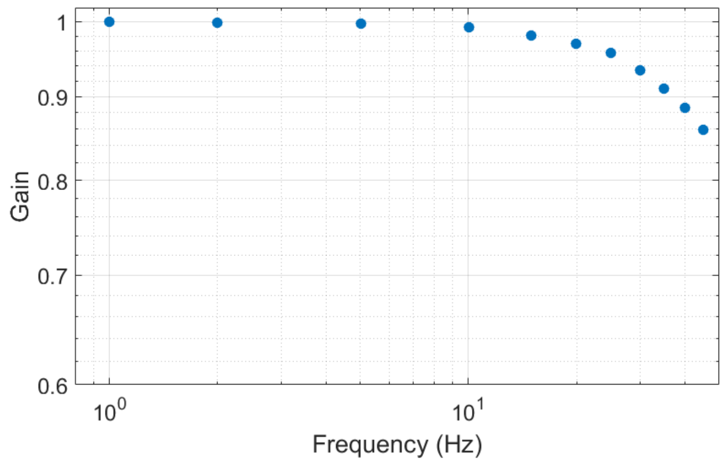

Figure 12 Bandwidth of the probe DC based polar angle measurement.

b. Characterization of the Light-shift Method

A small 3 kHz dither signal is applied to the laser current and modulates the wavelength of the laser light. This introduces a light shift that can be used for the polar angle measurement. The magnetometer reading is demodulated at 3 kHz with a bandwidth of 36 Hz. The Y component of the demodulator is then reported by the MFAM sensor.

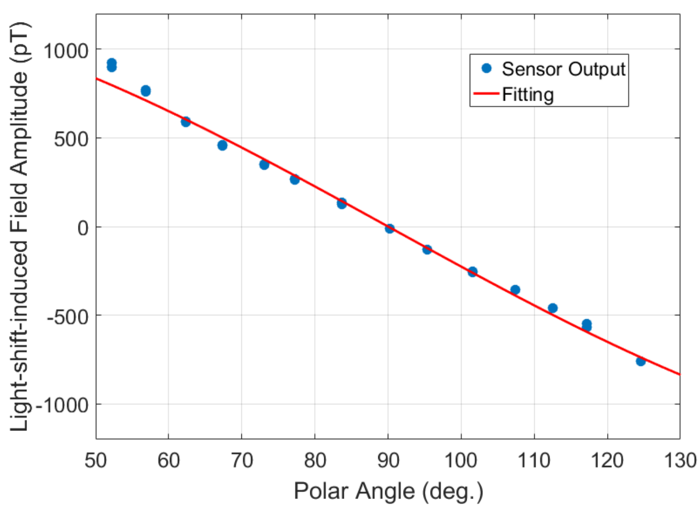

Figure 13 Amplitude of the light-shift-induced oscillating field as a function of polar angle (blue dots). The red curve is a fit of a cosine function to the data.

We first investigate the Y component amplitude as a function of the polar angle. The data is shown in Figure 13 as blue dots. A fit of a cosine function to the data is shown as the red curve. The data is well represented by a cosine curve around polar angles close to 90°, which is where the probe DC method is least sensitive. Away from 90°, only the sign of the Y component is used.

The Allan deviation is also measured and shown in Figure 14. With an integration time of about 100 ms, the noise in the demodulator Y component output is about 40 pT. The slope of the curve in Figure 13 is about 0.05 degree/pT around 90° polar angle, which yields a resolution of about 2° for the light-shift based polar angle measurement.

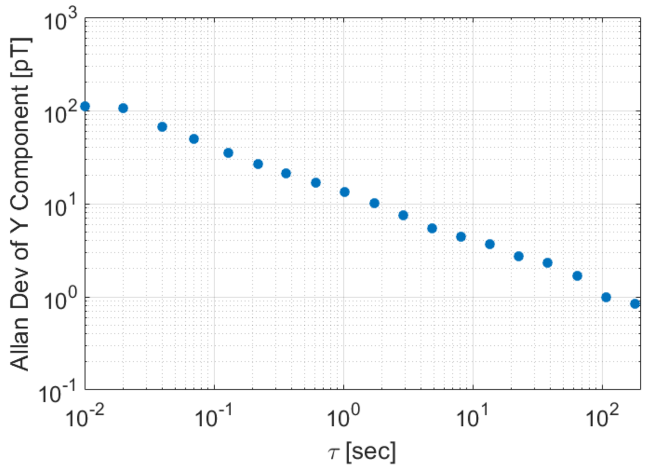

Figure 14 Allan deviation of the amplitude of the light-shift-induced oscillating field.

This is much worse than the sensitivity achieved with the benchtop setup. It is mostly due to the linewidth of the VCSEL lasers, which is typically around 100 MHz, compared sub-MHz linewidth for the DBR lasers used in the benchtop magnetometer. The signal to noise ratio is thus reduced by about a factor of 10 due to the VCSEL linewidth.

c. Measurement of the Polar Angle

We combine the probe DC method and the light-shift method to generate the final polar angle. The measured probe DC is first compared with the minimum value in the lookup table. If it is within 5 mV from the minimum, the polar angle is calculated as the arccosine of a/A, where a is the demodulator output and A is the amplitude of the fitting cosine function shown in Figure 13. For other values of probe DC, the polar angle, θ, is first calculated according to the lookup table. Then, based on the sign of a, the polar angle is decided between θ and 180° - θ.

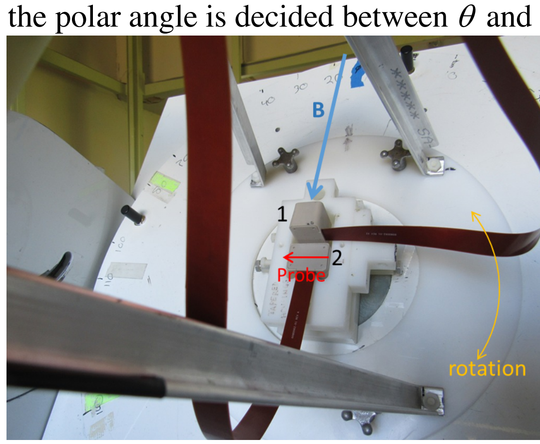

Figure 15 Testing setup for the polar angle measurement.

We have installed a test setup in a facility at a location where the Earth magnetic field is minimally disturbed. The sensors are mounted to a rotation table, as shown in Figure 15. The optical axis of the sensor 1 is aligned with the rotation axis of the table and the sensor 2 optical axis lies parallel to the rotation plane. The rotation angle of the table is recorded by an optical encoder with a sensitivity of 0.35°. The rotation plane can also be adjusted between -30° and 70° with respect to the Earth magnetic field.

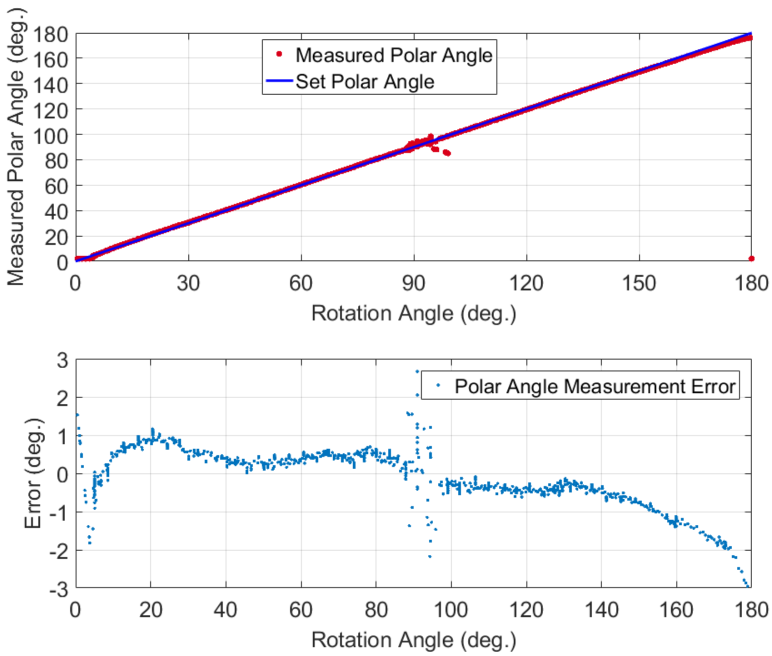

Figure 16 Top: the measured polar angle vs the set polar angle. Bottom: the difference between the measured polar angle and the set polar angle vs the set polar angle.

To test the polar angle measurement of the sensor 2, the table is set up such that its rotation axis is perpendicular to the Earth magnetic field. In this configuration, the rotation angle of the table (with a constant offset depending on the zero-angle position) is the set polar angle of the sensor 2. We record both the measured polar angle and the optical encoder output and plot the measured polar angles as a function of the set polar angle in Figure 16 (top). The difference between the measured polar angle and the set polar angle is also plotted in Figure 16 (bottom). As seen, for polar angles from 20° to 160°, the measurement produces fairly accurate results except in the vicinity of 90° where only the light-shift method is used.

2. Azimuthal Angle Measurement

As discussed in Section 1, with two sensors, the azimuthal angle can also be measured. We set up two nearly orthogonal sensors as shown in Figure 15, with the sensor 1 optical axis defining the z-axis and the sensor 2 optical axis as the x-axis. In such a coordinate system, the polar angle of the sensor 1 defines the polar angle of the system and the azimuthal angle is calculated according to Equation (3). The system polar angle is set by adjusting the rotation plane angle with respect to the Earth magnetic field with an accuracy of about 1°. At a set polar angle, the table is rotated with the optical encoder output measuring the azimuthal angle. We define the total angle measurement error as the square root of sum of squares of polar and azimuthal errors. For a set polar angle between 60° and 160° in steps of 10° and a set azimuthal angle from 0° to 180° in steps of 5°, the total angle measurement error is plotted on a color scale from 0° to 6° in Figure 17. The scale saturates at 6°. As seen, the angle measurement method can produce results better than 3° accuracy for most orientations. The error goes up significantly when one sensor approaches its dead zone, where its optical axis is aligned with the magnetic field. This is not surprising since at the center of the sensor dead zone, both the probe DC method and the light-shift method fail to produce the polar angle.

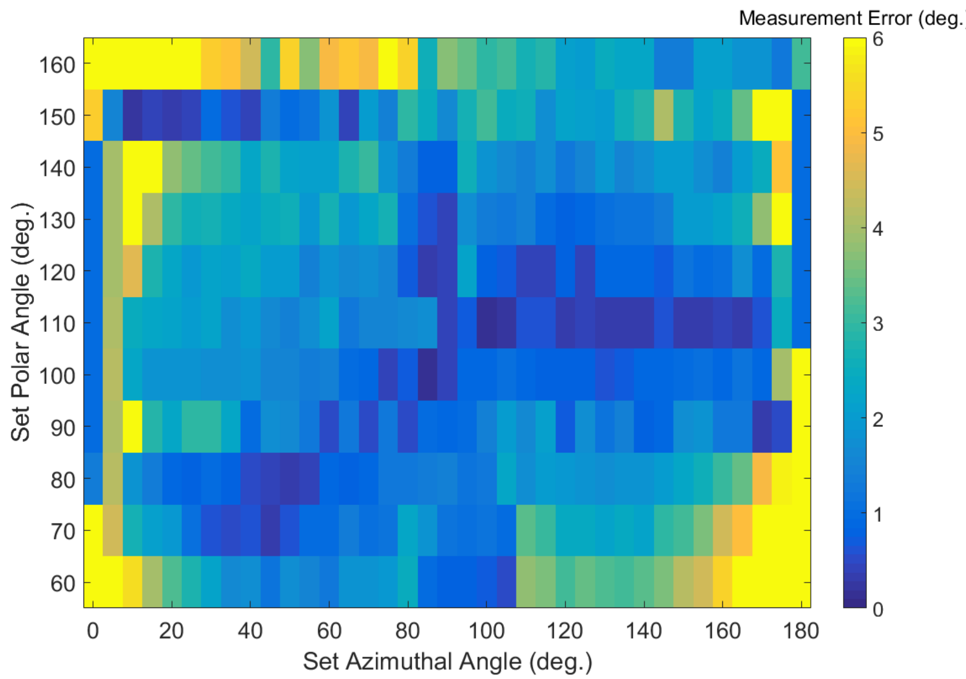

Figure 17 Total angle measurement error at different set angles.

3. Discussion

The biggest challenge facing the angle measurement is the stability of the operating temperature of the atomic vapor cell. A diode next to the cell is used to stabilize the cell temperature. However, the operating temperature of the cell is set by its coldest point, which is not necessarily detected by the diode. Change of the environmental temperature can affect the cell operating temperature slightly, leading to shape changes in the probe DC signal vs the polar angle curve, as shown in Figure 10. In fact, if we use two different lookup tables, one for a higher cell temperature, a much better measurement accuracy can be achieved.

The sensitivity in the light-shift method cannot be improved much due to the limit of the VCSEL lasers. With future improvements in VCSEL fabrication technology, the light-shift method can also be improved. In the azimuthal angle measurement, at present, there is still an ambiguity between azimuthal angle, φ and 360°- φ. If the pump and the probe lights have an angular separation, the phase delay of the Larmor signal with respect to the pumping signal becomes dependent on the rotation of the optical plane defined by the pump and the probe beams. In principle, this phase delay can be used to remove the ambiguity in the azimuthal angle measurement. The implementation of this method is beyond the scope of the current research.

Conclusions to Date

In conclusion, we have demonstrated the measurement of orientation of the magnetic field using a scalar atomic magnetometer with advanced signal extraction techniques. Away from the dead zones and 90° polar angle, a single sensor can measure the polar angle to better than 1° in accuracy and 0.1° in precision with 100ms integration time. With two orthogonal sensors, the azimuthal angle of the field can also be measured with an accuracy of better than 10°. The accuracy of the angle measurement method is sufficient to achieve the Tasks 2 and 3 objectives.

We emphasize that the 100 Hz sample rate reported herein only pertains to the angle measurement. The magnetic field output sample rate of the magnetometer itself is 1 kHz. In practical applications, the angle measurement is used to mitigate the effects on the magnetometer operation of changes in the relative orientation of the integrated system with respect to the Earth's magnetic field. An angle reporting rate of 100 Hz should be sufficient for this purpose.

In practical surveys, the MFAM-TDEM system will not change its relative orientation significantly with respect to the Earth field in less than 100ms. Hence, an Earth's field orientation measurement lasting as short as 100ms can be interleaved with the TDEM pulse sequence and enhance the system capabilities by enabling magnetic field measurement during the TDEM pulse. In this scenario, even with an angle measurement error of 10°, the resulting error in the estimated Larmor frequency during the EM pulse would be less than 1 kHz. This is less than the FWHM of the typical magnetic resonance in the scalar magnetometer and should enable the fast recovery of the magnetometer operation during the EM pulse.

In many applications, we are only interested in the magnetic field after the EM pulse is turned off. To addresses those cases, we have investigated in Task 2 fast-recovery methods that do not rely on the angle measurement. Under the real-world field conditions, we do expect the angle measurement to be less robust mainly due to the temperature fluctuation in the environment. This issue can be addressed by using additional thermally insulating materials covering the sensor.

Any field measurement during the EM pulse requires a significant local compensation of the EM pulse at the location of the magnetometer. Otherwise the heading error will most likely dominate the measurement for any practical applications. The compensated local EM pulse is likely to be less than one microtesla, as investigated in Task 3. For a practical MFAM-TDEM system, the vector field produced by the transmit coil at the location of the MFAM can be initially calibrated and will not vary during the survey. In this case, only the orientation of the Earth's magnetic field relative to the sensors needs to be determined.

Some of the questions in system integration when using the Advanced MFAM Sensors with TDEM systems will be in understanding the tradeoffs between triggered measurement and continuous measurement, merging short-time data from pick-up coil sensors and long-time data from magnetometers, and compensating the field from the primary pulse-generating coils.

Literature Cited

1] D. Budker, and D. F. J. Kimball, Optical Magnetometry, Cambridge: Cambridge University Press, 2013.

2] W. E. Bell, and H. L. Bloom, "Optically driven spin precession," *Phys. Rev. Lett.* , vol. 6, p. 280, 1961.

3] D. W. Allan, "Statistics of Atomic Frequency Standard," *Proceedings of the IEEE,* vol. 54, no. 2, pp. 221-231, 1966.

4] H. Tang, W. Happer, and B. S. Mathur, "Light shifts in the alkali atoms," *Phys. Rev.*, vol. 171, p. 11, 1968.